Molecular Cell *23*, 913–923, September 15, 2006 ©2006 Elsevier Inc. DOI 10.1016/j.molcel.2006.07.020

Large Conformational Changes in a Kinesin Motor Catalyzed by Interaction with Microtubules

Keiko Hirose,[1,4,*] Erika Akimaru,[1] Toshihiko Akiba,[1,5] Sharyn A. Endow,[2] and Linda A. Amos[3]
[1] Gene Function Research Center
National Institute of Advanced Industrial Science and Technology
Tsukuba, Ibaraki 305-8562
Japan
[2] Department of Cell Biology
Duke University Medical Center
Durham, North Carolina 27710
[3] MRC Laboratory of Molecular Biology
Cambridge, CB2 2QH
United Kingdom

Summary

Kinesin motor proteins release nucleotide upon interaction with microtubules (MTs), then bind and hydrolyze ATP to move along the MT. Although crystal structures of kinesin motors bound to nucleotides have been solved, nucleotide-free structures have not. Here, using cryomicroscopy and three-dimensional (3D) reconstruction, we report the structure of MTs decorated with a Kinesin-14 motor, Kar3, in the nucleotide-free state, as well as with ADP and AMPPNP, with resolution sufficient to show α helices. We find large structural changes in the empty motor, including melting of the switch II helix α4, closure of the nucleotide binding pocket, and changes in the central β sheet reminiscent of those reported for nucleotide-free myosin crystal structures. We propose that the switch II region of the motor controls docking of the Kar3 neck by conformational changes in the central β sheet, similar to myosin, rather than by rotation of the motor domain, as proposed for the Kif1A kinesin motor.

Introduction

The kinesin motors form a large family of related proteins that use ATP to move along MTs, performing essential functions in cellular transport and cell division. Despite several decades of work, the mechanism by which motor proteins use ATP to move along their cytoskeletal filament is not understood. The motors are thought to couple steps of ATP hydrolysis to conformational changes in the motor domain, or head, and interactions of the motor with MTs to generate force for movement. One approach to understanding the motor mechanism is to identify the structural changes of the motors that occur when the motor is bound to different nucleotides. The nucleotide states that have been characterized in biochemical and structural studies are those in which the motor is bound to ADP, no nucleotide, or the ATP analog AMPPNP. These nucleotide states are thought to represent steps in the hydrolysis of ATP by the motor.

Crystal structures of the motor domains of Kinesin-1 (conventional kinesin) and kinesin-related proteins show conformational changes that depend on the nucleotide bound to the motor. Key motor elements that move in different nucleotide states include switch I and II, motifs that are structurally homologous to myosin and G protein regions that move upon nucleotide hydrolysis and exchange (Vale and Milligan, 2000; Sablin and Fletterick, 2001; Kull and Endow, 2002). The observed changes include movement of switch I and II closer to the bound nucleotide in the ATP-like state, and changes in length and rotation of the switch II helix α4 together with the adjacent loops and helix (Kikkawa et al., 2001; Nitta et al., 2004; Yun et al., 2001). Rotation of the switch II region has been proposed to control interactions of the head with the adjacent neck that result in directional movement of the kinesin motors along the MT. An outstanding question that remains is which of these structural changes underlies force production by the kinesin motors.

The major difficulty in determining a possible mechanism for kinesin motility from X-ray crystal structures is that the available structures are solved in the absence of MTs, as efforts to obtain motor-tubulin crystals have not yet been successful. Because the kinesin motors show a striking increase in the rate of ATP hydrolysis in biochemical assays when MTs are added, the structure of the motors is expected to change dramatically upon binding to MTs. In order to study the structure of the kinesin motors bound to MTs, cryomicroscopy and computer reconstruction methods have been used. The 3D maps of kinesin proteins complexed with MTs in the presence of different nucleotides have shown that a kinesin head bound to ADP, no nucleotide, or an ATP analog binds to essentially the same site on MTs (Hirose et al., 1995; Hoenger et al., 1998, 2000). When dimeric kinesin constructs were analyzed, the second head changed position depending on the nucleotide present (Arnal and Wade, 1998; Hirose et al., 1998, 1999, 2000). However, the resolution of the structures in these previous studies was not high enough to identify the changes that occur with different nucleotides in the MT-bound head of the motor.

A large conformational change of an MT-bound kinesin motor was reported by Kikkawa et al. (2001) analyzing a monomeric, plus-end-directed Kinesin-3 motor, Kif1A. By cryomicroscopy, they reported an ~20° rotation of the Kif1A head bound to MTs in the presence of ADP, relative to AMPPNP. The observed structural changes were interpreted to correspond to the rotation of the switch II helix α4 between the ADP- and ATP-like forms of Kif1A. When the motor is bound to an MT, the switch II helix is thought to be fixed in position on the MT, so that the rest of the head rotates. However, 3D structures of the MT-bound Unc104 motor, which belongs to the same Kinesin-3 subfamily as Kif1A, showed a rotation of less than five degrees between the ADP and

*Correspondence: k.hirose@aist.go.jp
[4] Present address: Research Institute for Cell Engineering, AIST, Tsukuba, Ibaraki 305-8562, Japan.
[5] Present address: Biological Information Research Center, AIST, Tsukuba, Ibaraki 305-8566, Japan.

AMPPNP states (Al-Bassam et al., 2003). Because almost all of the crystal structures of the kinesins reported so far are bound to ADP, we do not know whether a rotation of the head occurs in other kinesin motors.

A second unknown factor is the high-resolution structure of nucleotide-free kinesin motors, which has been difficult to study by crystallography because many kinesin proteins denature in the absence of nucleotides or MTs. Recently, the crystal structure of a Kinesin-13 subfamily member, KinI, without nucleotide was reported (Shipley et al., 2004). However, the nucleotide pocket contained a sulfate ion, and its conformation resembled the ADP structure. Therefore, it is unlikely that this structure represents that of kinesin bound to an MT without nucleotide.

Here, using cryomicroscopy and 3D computer reconstruction methods, we have analyzed a kinesin motor bound to MTs without nucleotide as well as with ADP and the ATP analog AMPPNP at an unusually high resolution that is sufficient to show α helices. As the kinesin motor, we used Kar3, a Kinesin-14 motor protein that moves toward the MT minus end and shows MT-depolymerizing activity (Meluh and Rose, 1990; Endow et al., 1994). Our results reveal that the nucleotide-free state is significantly different from any of the crystal structures and show a change involving melting of a key element of the motor, the switch II helix α4, at the MT binding interface, which has not been observed previously. We propose that structural changes in switch II control interactions of the Kar3 head with its neck and are transmitted via changes in the central β sheet of the motor, similar to myosin (Coureux et al., 2003; Reubold et al., 2003), rather than a rotation of the motor domain, as proposed for Kif1A.

Results

Cryomicroscopy and 3D Reconstruction

We studied MTs decorated with the monomeric Kar3 motor domain in three states: (1) bound to ADP, (2) without nucleotide (empty), or (3) bound to the ATP analog AMPPNP (ATP-like). In the absence of nucleotide, all the MTs looked fully decorated and the diffraction patterns showed strong 80 Å layer lines, indicating a high degree of order (Figure S1.1 in the Supplemental Data available with this article online). In the presence of ADP or AMPPNP, the decoration seemed to be weaker. Some MTs were only partially decorated with Kar3, especially with ADP, which causes the motor to bind weakly to MTs. However, motor decoration of MTs in the presence of ADP was better than in our previous studies (Hirose et al., 1995), and we were able to select images of a similar quality for all three states.

The averaged 3D density maps showed structures with a much higher resolution than we had obtained previously (Hirose et al., 1998, 2000). Fourier shell correlation plots (Figure S1.2A) show that the agreement between independent sets of averaged data is above theoretical critical background levels (Frank et al., 1996), corresponding to good resolution, especially in the longitudinal direction (see below). Two-dimensional plots of the layer-line data (Figure S1.2B) also show that there is significant signal for the layer lines down to 10 Å. We think the improvement in resolution is due to the use of an electron microscope (EM) with a field emission gun and the careful alignment procedure developed by Toyoshima (2000), the correction for the contrast transfer function (Tani et al., 1996) that we applied, and the unusually tight binding of Kar3 to MTs even in the weakly bound ADP state. Previous kinetic measurements show the Kar3-MT dissociation constants to be relatively low, indicating tight binding to the MT. The apparent K_d values of the motor from MTs were 1.7 ± 0.7 μM with ADP and 0.19 ± 0.08 μM with no nucleotide (Song and Endow, 1998), and 0.77 ± 0.25 μM with AMPPNP (H. Song and S.A.E., unpublished data). The K_d values determined for the Kar3 protein used in the present experiments were not significantly different from those reported previously, again consistent with tight binding by the motor to MTs.

The cryomicroscopy surface maps of Kar3-MTs showed features corresponding to loops and some α helices of Kar3 and tubulin, which we could identify by comparison to atomic structures (Figure 1). The undecorated MT (Figure 1A) and MTs for the three motor-MT states (Figures 1B–1D) looked similar, indicating that the detailed features in the density maps are not noise. They are also similar to a model structure calculated from the tubulin crystal structures (Löwe et al., 2001) with the resolution lowered to 10–12 Å (Figure S2.1), indicating that the resolution of our 3D maps is ~12 Å or higher. The maps typically have their best resolution along the helix axis and include sufficient high-resolution signal to reveal key α helices of the motor, such as helix α4. The resolution in radial and transverse directions is lower but is sufficient to show exposed tubulin surface helices, like H11 and H12.

Docking of Crystal Structures into the 3D Maps

The 3D maps show that Kar3 heads bind to essentially the same position on MTs as observed previously for other kinesin family motors, interacting with both α- and β-tubulin (Figure 1). Although the overall orientation of the heads appears similar for all three states, protrusions on the surface of the head, corresponding to various loops, differ in position in the three maps, indicating that the loops move when the motor is bound to different nucleotides. The top of the head also seems flatter in the empty state (Figure 1C), presumably due to movements of structural elements in the motor. In order to investigate the structural changes in more detail, we docked α- and β-tubulin crystal structures into the density maps together with a crystal structure of Kar3.

The 3D maps with the docked crystal structures are shown in Figures 2–5 with a longitudinal view in Figure 2, cross-sections in Figures 3 and 4, and sections through the Kar3 nucleotide binding pocket in Figure 5. The tubulin crystal structures (1JFF.pdb; Löwe et al., 2001) fit very nicely into the density maps. Some of the α helices, e.g., H3 and H4, are resolved as cylinders of high density (Figure S2.2). On the outer surface of the MTs, helices H11 and H12 of α- and β-tubulin are clearly visible (Figures 1 and 2 and Figure S2.2). There is extra density corresponding to the C terminus of α-tubulin (Figures 1 and 2, green arrowheads), which is not present in the crystal structure. In both decorated and undecorated MTs, the density of the C terminus of β-tubulin (Figure 1, yellow

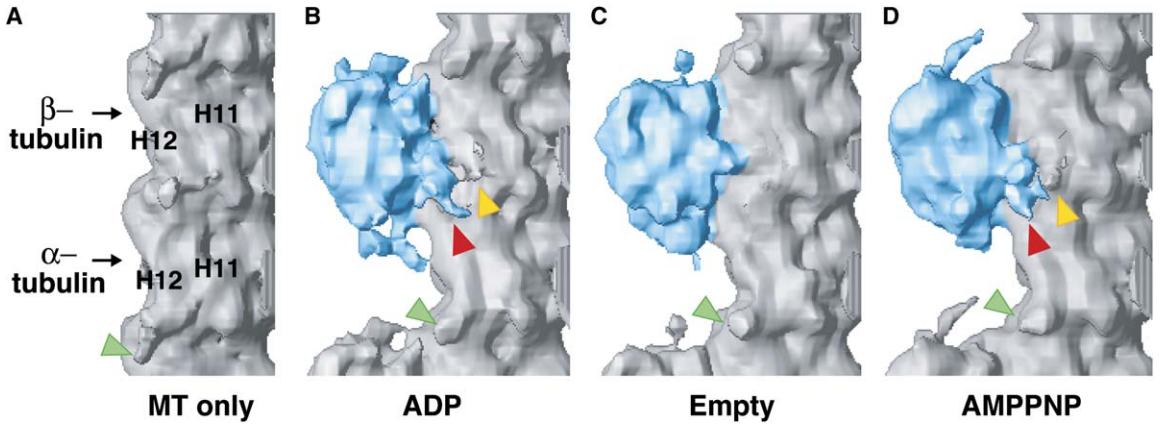

Figure 1. Surface Maps of the 3D Density

(A–D) Three-dimensional maps of undecorated MTs (A) and MTs decorated with Kar3 in the ADP (B), empty (C), and AMPPNP (D) states. Side view rotated 53° from the front view shown in Figure 4D, with the plus end at the top. Density corresponding to the Kar3 head is cyan. (B–D) A large protrusion is present on the right side of the head ([B] and [D], red arrowheads), corresponding to Kar3 loop L12, which is absent in the empty state (C). The C termini of α-tubulin (green arrowheads) and β-tubulin (yellow arrowheads) are indicated, and helices H11 and H12 are labeled.

arrowheads) is weaker than that of α-tubulin, suggesting that the C terminus of β-tubulin is more mobile.

We also docked a crystal structure of the Kar3 motor into the density maps. Because all the crystal structures of Kar3 that have been reported are bound to ADP, we docked a Kar3-ADP structure (1F9T.pdb; Yun et al., 2001) into the EM maps of all three nucleotide states, fitting it by eye. The Kar3 motor domain, like that of other kinesin proteins, consists of a central eight-stranded β sheet (arrow) flanked by three α helices to each side (Figure 2D). The nucleotide binding cleft lies at the end of an α helix on the side of the motor facing away from the MT, whereas the MT binding region comprises two α helices, α4 and α5, with their adjacent loops, L11 and L12, on the opposite side of the motor, facing the MT. Switch II consists of loop L11, which is largely disordered in the Kar3 crystal structure and not visible in the view shown in Figure 2D, and helix α4. Switch I consists of helix α3-loop L9-helix α3a toward the back of the motor from the view shown in Figure 2D (see Figure 3D).

The crystal structure of Kar3-ADP fit best when it was in essentially the same orientation in each map (Figure 2 and Figure S3). As previously reported, the switch II helix α4, which is important for motor binding to the MT, is approximately perpendicular to the MT axis and is situated in the α-β-tubulin intradimer groove (Figure 2). The Kar3 crystal structure also fit well into the high-density region of the maps alone (Figure S3), indicating that the high density corresponds to the structural elements of the motor core. Nucleotide-dependent rotations of the MT-bound motor in our maps were within several degrees, contrasting with reports by others of a large rotation between nucleotide states (Kikkawa et al., 2000, 2001).

Difference maps showed positional differences in positive and negative density but no large-scale differences, indicating that rigid body movement is not detectable at this resolution. The changes observed between the maps appear to involve rearrangement of individual structural elements such as α helices, β strands, and loops. Major changes were observed in the position or shape of density corresponding to the Kar3 switch I and II regions, including the MT binding site and extending to the central β sheet and the nucleotide binding pocket.

Conformational Changes in the Switch I Region

Large structural changes were observed in the switch I region, as seen in a cross-section taken through the Kar3-MT maps (Figure 3). Switch I helix α3a and L9 do not fit well into the EM density in any of the maps, indicating that the structure of this region in all three states is different from the Kar3-ADP crystal structure. Instead, there is an extra peak of density closer to tubulin in the empty state (Figure 3B, cyan arrowhead), evidence of a large structural change with the switch I region moving closer to α-tubulin. This region includes switch I and II residues that form a salt bridge in some crystal structures (Sack et al., 1999). These changes are also seen in the averaged data without sharpening (Figure S4), indicating that they are accurate representations of the density changes in the maps. Difference maps between states of the same sections as Figure 3 show the increased density of the switch I region in the empty state compared to the ADP and AMPPNP states (Figure S5).

Two crystal structures of Kar3 mutants have been reported that show large conformational changes in switch I (Yun et al., 2001). Attempts to fit one of these structures into the nucleotide-free Kar3-MT density map showed a better fit in the switch I loop L9 region than the wild-type Kar3 structure, but none of the crystal structures fit well into the switch I helix α3 region of the EM map. These differences indicate that structural changes in switch I occur in MT-bound motors that have not yet been observed in crystal structures.

Conformational Changes in the Switch II Region

Large changes in the motor with different nucleotide states are also observed in switch II loop L11-helix α4 and the following loop, L12. Switch II helix α4 in the kinesin crystal structures shows variable length, especially at its N terminus, depending on the nucleotide state (Kikkawa et al., 2001; Nitta et al., 2004) or on mutation (Yun et al., 2001). The Kar3 structure we used for

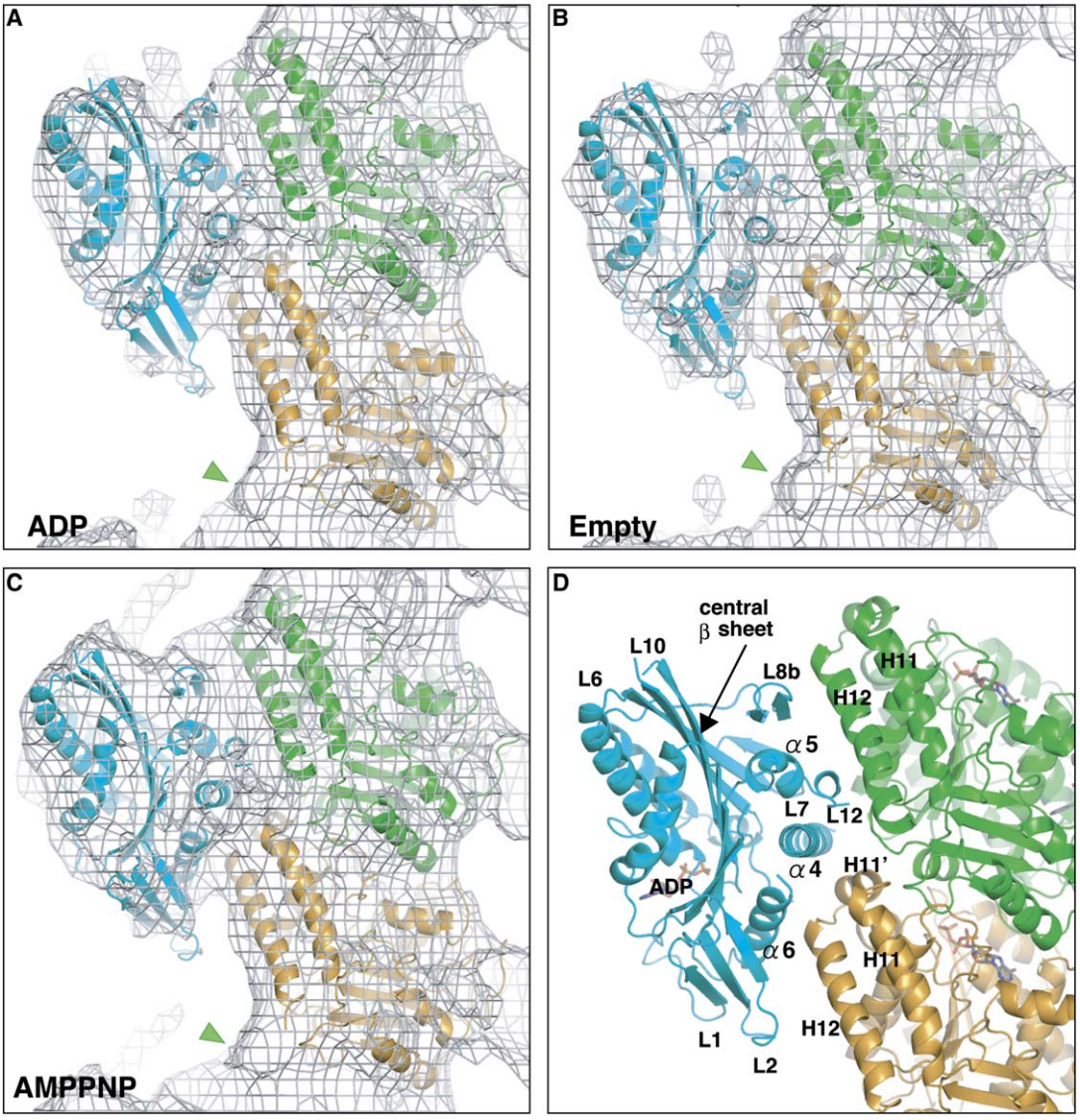

Figure 2. Kar3 and Tubulin Crystal Structures Docked into the EM Maps

(A–C) Kar3-MT 3D maps in the ADP (A), empty (B), and AMPPNP (C) states, with the crystal structures of Kar3 (cyan), α-tubulin (gold), and β-tubulin (green) docked into the density. The maps are rotated around the MT axis by 65° from the front view, with the MT plus end at the top, and viewed longitudinally. The EM density maps are represented as a surface net (gray mesh). Density attributed to the C terminus of α-tubulin is indicated by green arrowheads.

(D) Motor and tubulin crystal structures shown as ribbon diagrams with key structural elements labeled. ADP bound to the motor, GTP bound to α-tubulin, and GDP bound to β-tubulin are shown as wire-frame models.

docking has a very long helix α4 with only the N terminus of the preceding switch II loop L11 visible (Yun et al., 2001). When docked into the EM density, the N terminus of helix α4 (near the α4 label in Figure 3C) extends out of the high-density envelope (red mesh) in the ADP and AMPPNP states (Figures 3A and 3C), suggesting that the helix unfolds and makes a longer loop, L11. In the empty state (Figure 3B), the N terminus of helix α4 partly overlaps the high-density envelope but the density is not observed as a separate cylinder, again indicating a conformational change in the N terminus of helix α4. Longitudinal sections show a connection between density attributed to loop L11/helix α4 and α-tubulin (Figure S6, black arrowheads). The density is greater in the empty and AMPPNP states than in the ADP state. These results indicate that the N terminus of helix α4 melts and interacts with α-tubulin in all three states, but the interaction appears stronger in the empty and AMPPNP states.

Loop L12 at the other end of helix α4, the C terminus, is missing from the Kar3 crystal structure, presumably because it is mobile. However, a projection of weak density is present in the motor-MT ADP and AMPPNP maps in the position expected for loop L12 (Figures 1 and 3, red arrowheads). The density of this region is weak in the Kar3-MT structures, and we could not see a clear connection between L12 and tubulin resembling that reported for the Kif1A motor (Kikkawa et al., 2000; Okada and Hirokawa, 2000). However, the density attributed to loop L12 (red arrowheads) is positioned very close to the protrusion corresponding to the C terminus of β-tubulin

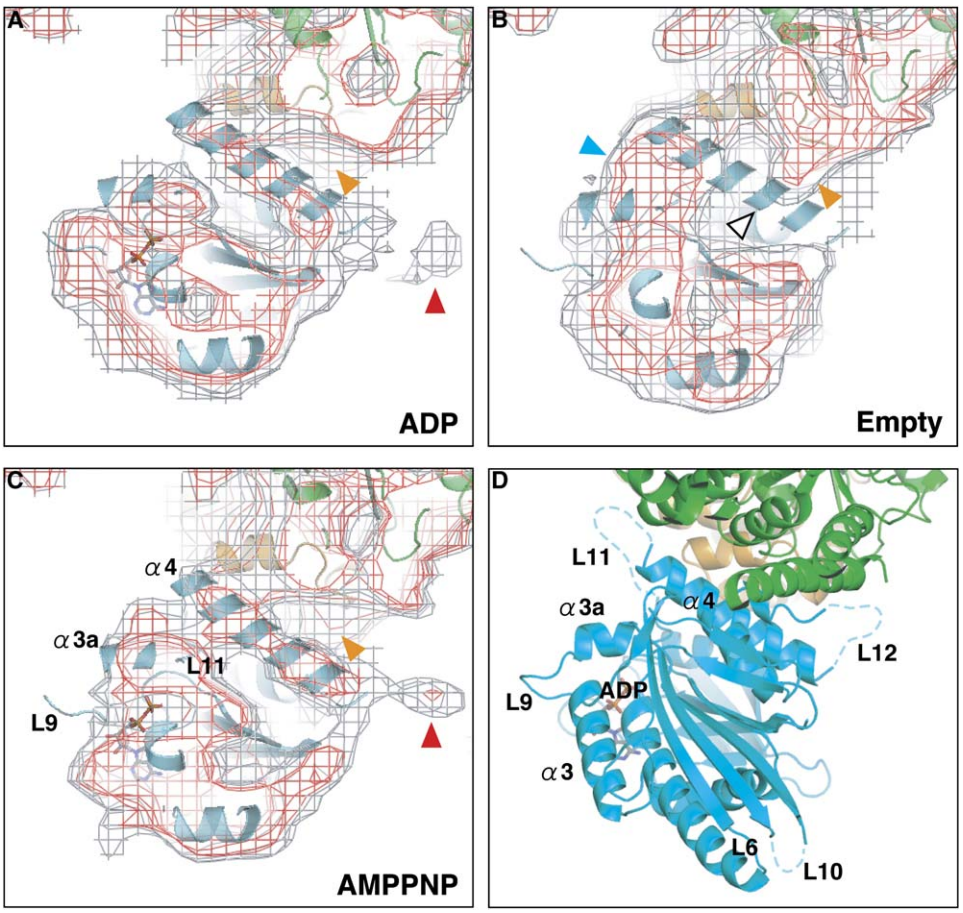

Figure 3. Changes in the Switch I and Switch II Regions

(A–C) Cross-sections of the Kar3-MT complex in the ADP (A), empty (B), and AMPPNP (C) states with the docked crystal structures, viewed from the MT plus end. The sections (10.7 Å thick) transect Kar3-MT near the midpoint of the motor (Figure 4D). Colors are the same as Figure 2 except that the maps are shown as high- (red mesh) and lower- (gray mesh) density levels. Nucleotide bound to Kar3 is not shown for the empty state. EM density corresponding to switch I changes in different states, indicating conformational changes ([B], cyan arrowhead). Density corresponding to switch II helix α4 no longer forms a distinct cylinder in the empty state ([B], white arrowhead). Density adjacent to tubulin, strong only in the empty state, may be the melted helix α4 (orange arrowheads). Extra density near the end of helix α4 may be loop L12 ([A] and [C], red arrowheads). (D) Motor and tubulin crystal structures shown as ribbon diagrams, viewed as in (A)–(C). Key elements are labeled, including switch I helix α3-loop L9-helix α3a and switch II helix α4. Only the ends of loops L10, L11, and L12, shown as dashed lines, are resolved in the Kar3 crystal structure. ADP bound to the motor is shown as a wire-frame model.

(yellow arrowheads) in the ADP and AMPPNP states (Figures 1B and 1D).

In the empty state, there is a dramatic structural change in the helix α4-loop L12 region. The projection corresponding to L12 is absent in the surface maps (Figure 1C). Thin sections show that helix α4 has disappeared as a distinct entity (Figure 3B, white arrowhead), and the density has moved to be continuous with tubulin. There is a region of high density near the end of helix α4 of the crystal structure that might correspond to the unfolded helix α4 and loop L12 (Figure 3B, orange arrowhead), which connects to helix H12 of β-tubulin and the top of α-tubulin. The corresponding regions in the ADP and AMPPNP states are low density (Figures 3A and 3C, orange arrowheads). These changes in density attributable to helix α4 are also observed in the unsharpened images (Figure S4) and in the difference maps between the sections (Figure S5), indicating that the density changes are present in the high-resolution data. Longitudinal sections that transect the motor near the C terminus of helix α4 of the crystal structure show that the density in this region is very weak in the empty state; instead, there is extra density in the groove between α- and β-tubulin (Figure S6, white and red arrowheads). These results are consistent with the interpretation that, in the empty state, helix α4 melts and interacts more closely with the MT in the intradimer groove.

Conformational Changes in the Central β Sheet

Another striking change observed in our 3D maps is the region including loop L7, a loop between strands β4 and β5, which form part of the central β sheet, on the surface facing the MT. Cross-sections near the top of the Kar3-MT maps show a large gap between loop L7 and the MT in the ADP and AMPPNP states (Figures 4A and 4C). However, in the empty state, the density attributable to loop L7 moves toward the MT and interacts with helix H4 of β-tubulin (Figure 4B, magenta arrowhead). At the same time, two loops, L6 and L10 (Figure 3D), on the

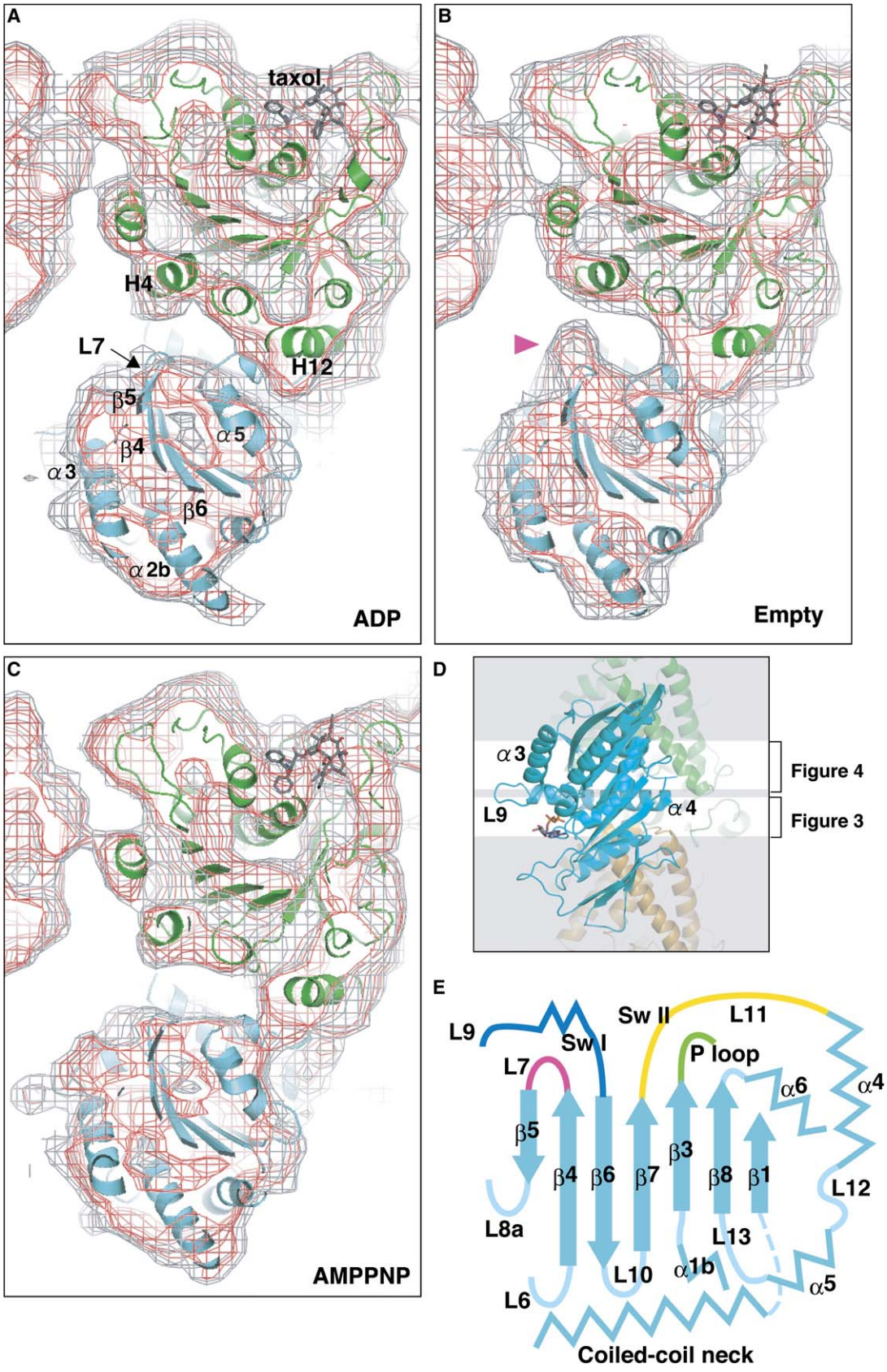
A
taxol
H4
L7
H12
β5
α5
β4
α3
β6
α2b
ADP
B
Empty
C
AMPPNP
D
α3
L9
α4
Figure 4
Figure 3
E
L9
Sw II
L11
Sw I
P loop
L7
α6
α4
β5
β3
β4
β6
β7
β8
β1
L12
L8a
L13
L10
α1b
α5
L6
Coiled-coil neck

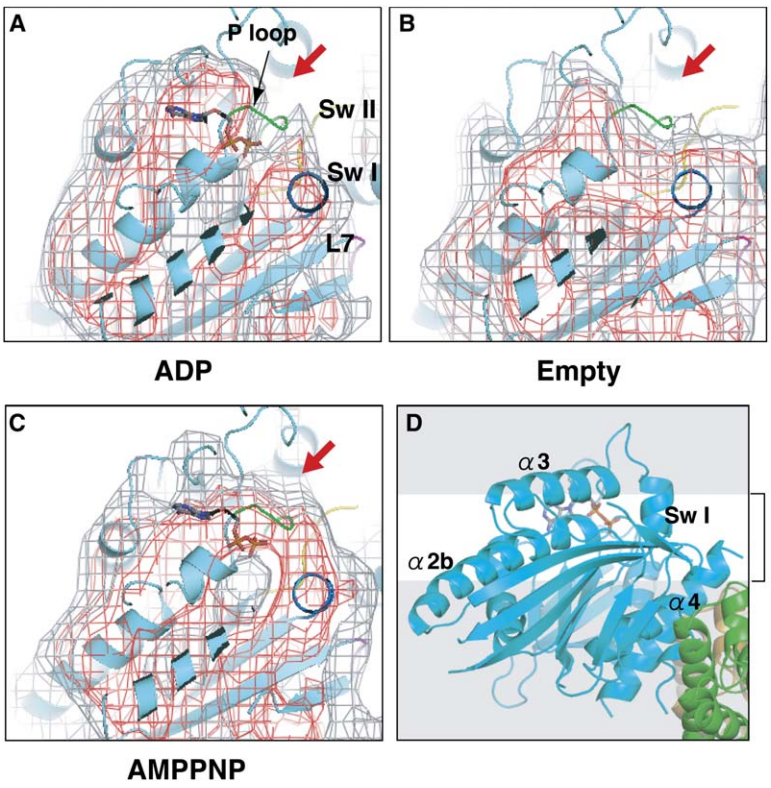

Figure 5. Changes in the Nucleotide Binding Pocket

(A–C) The nucleotide binding region in the Kar3-MT 3D maps (gray and red mesh) in the ADP (A), empty (B), and AMPPNP (C) states, with the Kar3-ADP crystal structure (cyan) docked into the density. Density corresponding to the Kar3 nucleotide binding pocket (red arrows) appears partially open in the ADP state (A), wide open in the empty state (B), and closed in the AMPPNP state (C). The P loop (green) of the Kar3 crystal structure, which forms the nucleotide binding cleft, is shown with bound nucleotide in the ADP and AMPPNP states but without nucleotide in the empty state. Switch I (Sw I, blue) and switch II (Sw II, yellow) are indicated, together with loop L7 (magenta) of the central β sheet.

(D) Motor and tubulin crystal structures shown as ribbon diagrams with the white region showing the level of the sections (14 Å thick). The viewing angle is similar to Figure 1 of Reubold et al. (2003), which shows the open and closed nucleotide binding pocket of myosin II.

other side of the Kar3 head change position, resulting in the flatter head observed in the no-nucleotide surface map (Figure 1C). Large shape changes of the Kar3 head depending on the nucleotide state can be seen in the thin sections and in the position of the density attributable to the central β sheet (Figure 4). These changes in density assigned to the central β sheet can also be seen in the high density only, which represents the structural elements of the motor core with well-defined density (Figure S3).

Crystal structures of myosin II and myosin V show that there is a rearrangement of the central β sheet when myosin goes into the nucleotide-free state, including the strands preceding the switch II loop, following switch I, and adjacent to switch I (Coureux et al., 2003; Reubold et al., 2003). These three β strands correspond to β7, β6, and β4 of the kinesins (Figure 4E). The large changes in position of density attributed to loop L7, a loop that connects strands β4 and β5, and the changes in shape and position of the density corresponding to the central β sheet between the ADP and empty states, make it very likely that a similar rearrangement of the β sheet occurs in Kar3 when it binds to an MT in the empty state. The present maps show evidence for such a rearrangement but do not reveal the structural changes in detail.

Changes in the Nucleotide Binding Pocket

The rearrangement of the central β sheet in myosin is caused by changes in switch I and II, which interact with nucleotide in the ATP-like state and move away from the nucleotide binding pocket or P loop in the nucleotide-free state, opening the pocket (Reubold et al., 2003). Although the resolution of our maps in the nucleotide binding region of Kar3 is not sufficient to show which loop moves, we can clearly see a cleft in the EM density corresponding to the nucleotide binding pocket (Figure 5, red arrows). The cleft is narrow in the ADP state, wide open in the empty state, and absent in the AMPPNP state. These results indicate that the nucleotide binding pocket is partially closed in the ADP state, opens when the motor loses nucleotide, and closes upon binding of ATP.

Discussion

Much effort has been devoted to determining the mechanism by which the kinesin and myosin motors use ATP

Figure 4. Conformational Changes in the Central β Sheet

(A–C) Thin sections of the Kar3-MT complex in the ADP (A), empty (B), and AMPPNP (C) states with the docked crystal structures, viewed from the MT plus end. Colors are the same as Figure 3. Tubulin crystal structures fit very nicely into the 3D map density in all three states, indicating that structural changes in tubulin are relatively small. α helices, especially those on the outer surface of the MT, are clearly resolved. Density corresponding to taxol (shown as a wire-frame model) is also visible. The cross-sections show changes in the position of density corresponding to loop L7 and β strands of the central β sheet. Density attributed to loop L7 moves toward helix H4 of β-tubulin in the empty state ([B], magenta arrowhead), causing changes in the density corresponding to the central β sheet.

(D) Motor and tubulin crystal structures showing the levels of the sections in Figures 3 (10.7 Å thick) and 4 (14 Å thick).

(E) Topology of the central β sheet and interconnecting secondary structural elements. The P loop is the conserved motif that forms the nucleotide binding cleft of the kinesin motors. Sw I, switch I; Sw II, switch II.

to produce force. Current models postulate that, as the motors interact with nucleotide and their filament, they undergo conformational changes that create internal strain, causing a recoil movement that produces force and a working stroke of the motor (Howard, 2001). The nature of the proposed force-producing conformational changes is not yet certain, although considerable interest has focused on the possibility that movements of the switch II helix (α4 of the kinesins or the so-called "relay" helix of myosin) represent key changes of the motors (Vale and Milligan, 2000; Sablin and Fletterick, 2001; Kull and Endow, 2002; Kikkawa et al., 2001; Nitta et al., 2004). It is also not clear how structural changes of the motors are coupled to steps of nucleotide hydrolysis and interactions of the motors with their filament. Here, we analyze high-resolution 3D maps of the Kar3 motor domain bound to MTs to identify the conformational changes the motor undergoes in different states of the ATP hydrolysis cycle.

The resolution of the Kar3-MT 3D maps that we report here is unusually high, allowing us to see changes in the motor at the MT binding interface as well as the central region of the motor and the nucleotide binding pocket that have not been observed previously. Although we cannot see all the changes that occur in different nucleotide states, which would require near-atomic resolution (e.g., 4 Å or higher), we do see key elements, such as helix α4, in the ADP and AMPPNP maps in the position expected from the crystal structure. We do not see it as a distinct object in the no-nucleotide map, even though the data are as good as for the other two states, indicating that there has been a significant change in the helix. Although we can reliably see this and several other major conformational changes in the MT-bound motor, at the present resolution, we cannot fully address the question of the consequences of the observed structural changes for nucleotide binding and catalysis by the MT-bound Kar3 motor.

Lack of Rotation of the Kar3 Head

The crystal structure of Kar3-ADP fits into our EM maps in essentially the same orientation with a difference of no more than a few degrees between maps. By contrast, Kikkawa and colleagues (Kikkawa et al., 2000, 2001) fit the Kif1A crystal structures into motor-MT maps so that helix α4 makes a similar contact with the MT but the bulk of the motor domain is rotated by 20° between the ADP and AMPPNP states. The Kif1A rotation is thought to be caused by breaking a salt bridge between switch I and the switch II loop L11 that serves as a latch to keep the motor core rotated in the strained "up" position before hydrolysis of ATP (Nitta et al., 2004). If so, the rotational angle of the motor relative to tubulin should depend on the conformation of loop L11, whose C-terminal end binds to tubulin. Because loop L11 is not very well conserved between different motors, the extent of rotation could vary between different motors.

Melting of Helix α4

Although Kar3 bound to MTs does not show detectable rotation, elements of the motor domain show large structural changes, especially in the nucleotide-free state. One of the most striking changes involves switch II loop L11-helix α4 and the adjacent loop L12. Upon binding to MTs in the empty state, helix α4 is no longer visible as a long helical structure, although density attributable to the element is present adjacent to its position in the ADP and AMPPNP maps. We interpret the changes in shape and position of the density to mean that the helix has unfolded into a loop, merging with the adjacent loop L12. A structural change of this magnitude in helix α4 has not been observed previously in any crystal structure of a kinesin motor, including a Kinesin-13 motor, KinI, crystallized without bound nucleotide (Shipley et al., 2004). Our results indicate that both the presence of MTs and absence of nucleotide are needed to observe the large structural changes in helix α4 seen here.

After melting, the C terminus of helix α4, which we believe now forms part of L12, binds to the groove between α- and β-tubulin. The main interaction is with the intradimer groove including the surface helices of α- and β-tubulin, rather than the C terminus of β-tubulin, as shown schematically in Figure 6. The interaction between the melted helix α4 and tubulin is expected to increase the binding affinity of the motor for MTs in the empty state.

The N terminus of helix α4 also seems to unfold to make a longer loop, L11, that interacts with α-tubulin and is represented by density that connects with tubulin. The connection is stronger in the AMPPNP and empty states than in the ADP state. Small changes in the length of helix α4 and loop L11 in crystal structures of the kinesin motors have been observed previously and interpreted as melting of the helix at the N terminus, increasing the length of loop L11 (Kikkawa et al., 2001; Nitta et al., 2004). Nitta et al. (2004) proposed that loop L11 in the AMPPNP state and loop L12 in the ADP state alternate in binding to MTs. Our results are consistent with their model in that binding of loop L11 is stronger in the AMPPNP state than in the ADP state.

Changes in the Central β Sheet

A second prominent change in the nucleotide-free map compared to the ADP map is the difference in position of the density corresponding to loop L7, which connects two strands of the central β sheet. We interpret the changes in position of loop L7 as a movement toward tubulin, which occurs together with changes in density attributed to the central β sheet. None of the crystal structures of kinesin motors reported so far show large changes in the central β sheet. However, recently published structures of myosin II (Reubold et al., 2003) and myosin V (Coureux et al., 2003) without bound nucleotide show distortion of the central β sheet, including the strands corresponding to β4, β6, and β7 of the kinesins. The new crystal structures are thought to resemble myosin bound to an actin filament in the rigor state. This conformation appears to be unstable without actin, but for myosin II, crystallization as a fusion protein with dynamin may have stabilized the conformation (Kull and Endow, 2004). A similar rearrangement of the central β sheet that can be observed only when stabilized by an MT may occur in the kinesin motors without bound nucleotide as indicated in Figure 6.

The central β sheet of the kinesins is connected to switch I and II by strands β6 and β7, respectively (Figure 4E). This means that changes in switch II helix α4 can cause changes in the central β sheet, which in

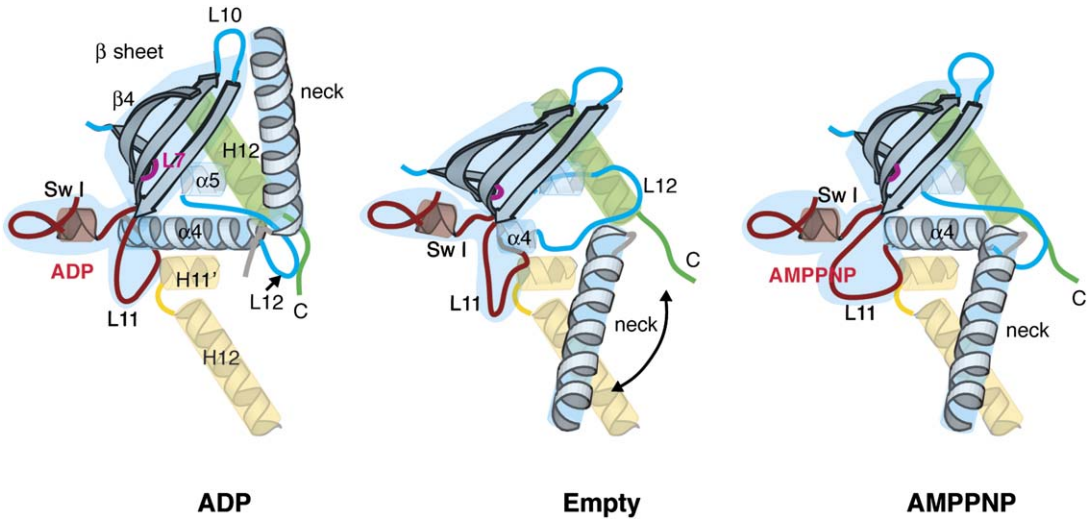

Figure 6. Kar3 Conformational Changes Catalyzed by MT Interactions

A model showing the consequences of movements by key Kar3 structural elements that undergo large conformational changes when the motor interacts with MTs. Helices H11′ and H12 of α-tubulin (gold) and H12 of β-tubulin (green) represent the MT. Kar3 (cyan) is shown with switch I (red), switch II loop L11 (red), and loop L7 (magenta). The neck, which is not included in the Kar3 crystal structures, is taken from an Ncd crystal structure (Yun et al., 2003). When the motor binds to an MT and loses ADP to form the empty state, the N terminus of switch II helix α4 melts, making a longer loop L11 that interacts strongly with α-tubulin and loop L7 moves toward the MT, along with strands of the central β sheet. This movement distorts the central β sheet and causes switch I to move, opening the nucleotide binding pocket. The C terminus of helix α4 melts, elongating loop L12, which interacts with tubulin, causing the motor to bind tightly to the MT. Distortion of the central β sheet also disrupts the interaction between the motor core, including loop L10, and the coiled-coil stalk or "neck." The neck is then free to rotate (double-headed arrow) and eventually becomes fixed in the direction pointing toward the minus end (as shown for the AMPPNP state), possibly as a result of other motor domains binding to new sites on the MT.

turn can affect the conformation of switch I and the nucleotide binding pocket near switch I. Although our EM maps do not resolve which of the nucleotide binding loops changes structure, the density corresponding to the nucleotide binding pocket clearly shows changes that agree with the interpretation that the pocket is partly open in the ADP state, wide open in the empty state, and closed in the AMPPNP state. Thus, the nucleotide binding pocket apparently opens when the motor binds to an MT and remains fully open after releasing nucleotide. Opening of the nucleotide pocket in the empty state is accompanied by distortion of the central β sheet.

A Structural Pathway for Kar3 Force Production

The structural changes of the kinesin motors that produce force are thought to involve interactions of the end of the coiled-coil stalk, which corresponds to the neck linker of plus-end-directed Kinesin-1, with the motor domain (Vale and Milligan, 2000). For Kif1A, the rotation of the switch II cluster allows docking of the neck linker in the AMPPNP state but prevents docking in the ADP state (Kikkawa et al., 2001). Ncd, a minus-end Kinesin-14 motor, like Kar3, has a coiled-coil neck that docks on the motor core in the Ncd-ADP crystal structure (Sablin et al., 1998; Kozielski et al., 1999). This has led to the proposal that rotation of the switch II region causes docking/undocking of the neck linker or neck of both the plus- and minus-end kinesin motors, but the movement is reversed in the minus-end motors (Kikkawa et al., 2001). Docking/undocking of the coiled-coil neck was observed in an Ncd crystal structure in which the neck was docked on only one of the heads and released from the other (Yun et al., 2003). The release of the neck from the undocked head was proposed to occur when the head releases ADP, although recent work has been interpreted to mean that it occurs when the bound head binds ATP (Wendt et al., 2002; Endres et al., 2006).

Docking/undocking of the neck is also likely to occur in Kar3. We looked for rotation of the Kar3 head in the motor-MT structures but found little or none, contrasting with the findings for Kif1A (Kikkawa et al., 2001). We cannot exclude the possibility that a small rotation sufficient to displace the neck occurs in Kar3 that was not detected in these studies or that the rotated conformation occurs transiently in Kar3 and is not seen in the three states we analyzed. A third possibility is that Kar3 uses a different mechanism to regulate docking/undocking of the neck. For Ncd, the coiled-coil neck interacts with motor elements on the opposite side of the central β sheet from the switch regions and loop L7 (Sablin et al., 1998; Figure 4E). Thus, the conformation of the central β sheet is likely to greatly affect the interaction between the neck and motor. The Kar3 construct we used here does not contain the neck, so we cannot tell which nucleotide state corresponds to the undocked state. However, the surface onto which the neck is expected to dock shows large changes, including movement of loops L6 and L10 between different nucleotide states. These large changes undoubtedly affect the interaction between the motor and the neck .

This leads to an attractive hypothesis. Rather than transmitting structural changes to the neck linker by rotation of the motor core, as in the KIF1A model, we speculate that changes in Kar3 in the MT binding region are transmitted through the central β sheet to the nucleotide binding site and the neck. When the motor binds to

tubulin, the N terminus of helix α4 melts, and the longer loop L11 interacts with tubulin (Figure 6). The structural changes in loop L11 lead to movement of loop L7, stabilized by interaction with β-tubulin. The movement of loop L7 distorts the central β sheet and moves switch I, opening the nucleotide binding pocket and releasing ADP. At the same time, the C terminus of helix α4 melts, extending loop L12 and its interactions with tubulin, causing the motor to bind tightly to the MT. The distortion of the central β sheet changes interactions between the neck and the motor core, which may allow the coiled-coil stalk to rotate, while the motor is most tightly bound to the MT. The empty head then binds ATP, the nucleotide binding pocket closes, and the C terminus of helix α4 winds up into a helix again, so that motor interactions with tubulin are less extensive than in the empty state. This weakens binding of the head to tubulin, preparing the motor for dissociation from the MT after ATP hydrolysis. Rotation of the coiled coil may occur after binding of ATP, as proposed recently by others (Endres et al., 2006), rather than immediately after ADP loss.

The interaction of L7 with tubulin and the subsequent distortion of the central β sheet are key steps in this model, driving the changes in the nucleotide binding pocket and neck. It could apply to other kinesins; as suggested by others, the same nucleotide-dependent movements in the plus- and minus-end-directed kinesins could have opposite effects on docking/undocking of the neck linker or neck. The rotation of the motor domain of Kif1A could be a secondary effect of helix α4 melting during nucleotide exchange and then refolding from its C terminus but could still serve a function. An interesting possibility is that processive motors such as Kif1A swivel between alternate conformations in order to bind to the next tubulin subunit. The proposal that the strain-producing conformational change that leads to force production is a distortion of the central β sheet in kinesins as well as in myosin provides a framework for further work defining the motor mechanism.

Experimental Procedures

Preparation of Kar3 and MTs

Kar3 protein corresponding to the conserved motor domain M-R384-K729 (38,912 Da) was expressed in *BL21(DE3) pLysS pArgU*$^+$ host cells by cell growth in M9ZB containing 5 μg/ml chloramphenicol, 5 μg/ml tetracycline, and 50 μg/ml ampicillin to OD_{550} of ~0.8, followed by addition of 0.4 mM IPTG and protein induction at 22°C for 5 hr (Gulick et al., 1998; Song and Endow, 1997). Protein was purified from the cell pellet through the SP-Sepharose step, as described (Song and Endow, 1997). Fractions from the SP-Sepharose peak were concentrated for use in EM or purified further by FPLC on Superose 12 before use. The concentrated purified protein in HEM100 (10 mM HEPES [pH 7.2], 1 mM $MgCl_2$, 1 mM EGTA, and 100 mM NaCl) was frozen in liquid N_2 and stored at −80°C.

Kar3 protein from the same purification as used for EM was tested for MT-stimulated ATPase activity and showed a V_{max} of 1.38 ± 0.04 s^{-1} and $K_{m,\ MTs}$ of 3.73 ± 0.14 μM. In tests for MT binding, the Kar3 protein showed a K_d of 0.37 ± 0.10 μM with no nucleotide and a K_d of 1.16 ± 0.21 μM with MgADP.

MTs were assembled from purified pig brain tubulin in a polymerizing solution (80 mM PIPES [pH 6.8], 1 mM EGTA, 5 mM $MgCl_2$, 1 mM DTT, 0.5 mM GTP, and 10% DMSO), stabilized with 20 μM taxol, centrifuged, and resuspended in a solution without GTP or DMSO.

EM

MTs diluted in MES solution (20 mM MES, 5 mM $MgSO_4$, 1 mM EGTA, 1 mM DTT, 10 μM taxol, pH 6.5–6.8) were applied to an EM grid coated with a holey carbon film, and Kar3 was added to give a final concentration of 10 μM. For freezing in the AMPPNP or no nucleotide states, the Kar3-MT mixture was mixed on the grids with 2 mM AMPPNP or 2 U/ml apyrase (final concentration) and then rapidly frozen by plunging the grids into an ethane slush. For the ADP state, the MT-Kar3 mixture was placed on a grid without nucleotide, and 1 mM ADP, 1 U/ml hexokinase, and 0.01% glucose were added just before freezing. The grids were examined by using a Gatan cold stage in a Philips Tecnai F20 electron microscope operating at 200 kV. The images were photographed with Kodak SO-163 film at 50,000× magnification with a defocus of 1100–2800 nm and digitized in 7 μm steps by using a Zeiss Phodis scanner.

Image Analysis

Images of MTs with 15 protofilaments were used for helical 3D reconstruction. MTs were selected first by their Moiré patterns (Ray et al., 1993) and then by the Fourier transform patterns. Three-dimensional structures were computed by using the programs developed by C. Toyoshima (Toyoshima, 2000). In brief, images of MTs were straightened, and the axial repeat distances were determined by autocorrelation. MT lengths of two repeat distances (~300 nm) were boxed and interpolated so that the layer lines registered exactly with the sampling raster. The repeat distance and tilt were further refined, and then the out-of-plane tilt and origin shift were corrected. Phases in the transform data from different images were adjusted to match, as well as possible, those of a reference image by allowing for an axial phase-origin shift and a rotation about the axis. Individual layer line data sets were corrected for contrast transfer function before averaging (Tani et al., 1996).

Sixty-two, forty-eight, and sixty-five data sets were averaged for calculating the final 3D maps of the Kar3-MT complex in the ADP, empty, and AMPPNP states, respectively. Layer-line data up to 9 Å resolution were included and weighted with a linear function ([1 + 40R], where the reciprocal radius R is measured in $Å^{-1}$) to sharpen the higher-resolution data. The effect is mainly cosmetic, as the density differences are clear without sharpening (compare Figure 3 and Figure S4). The atomic coordinates of Kar3 (Yun et al., 2001) and α- and β-tubulin (Löwe et al., 2001) were docked separately into the EM density maps. Docking was optimized visually by using the program O (Jones et al., 1991).

Supplemental Data

Supplemental Data include six figures and can be found with this article online at http://www.molecule.org/cgi/content/full/23/6/913/DC1/.

Acknowledgments

We thank Dr. C. Toyoshima for kindly providing us with the programs for helical 3D reconstruction. This work was supported by a Grant-in-Aid for Scientific Research on Priority Areas from the Ministry of Education, Culture, Sports, Science and Technology to K.H., a grant from the National Institutes of Health to S.A.E., Medical Research Council funding to L.A.A., and a Human Frontier Science Program grant to K.H., S.A.E., and L.A.A.

Received: March 12, 2006
Revised: May 15, 2006
Accepted: July 17, 2006
Published: September 14, 2006

References

Al-Bassam, J., Cui, Y., Klopfenstein, D., Carragher, B.O., Vale, R.D., and Milligan, R.A. (2003). Distinct conformations of the kinesin Unc104 neck regulate a monomer to dimer motor transition. J. Cell Biol. *163*, 743–753.

Arnal, I., and Wade, R.H. (1998). Nucleotide-dependent conformations of the kinesin dimer interacting with microtubules. Structure *6*, 33–38.

Coureux, P.D., Wells, A.L., Menetrey, J., Yengo, C.M., Morris, C.A., Sweeney, H.L., and Houdusse, A. (2003). A structural state of the myosin V motor without bound nucleotide. Nature *425*, 419–423.

Endow, S.A., Kang, S.J., Satterwhite, L.L., Rose, M.D., Skeen, V.P., and Salmon, E.D. (1994). Yeast Kar3 is a minus-end microtubule motor protein that destabilizes microtubules preferentially at the minus ends. EMBO J. *13*, 2708–2713.

Endres, N.F., Yoshioka, C., Milligan, R.A., and Vale, R.D. (2006). A lever-arm rotation drives motility of the minus-end-directed kinesin Ncd. Nature *439*, 875–878.

Frank, J., Radermacher, M., Penczek, P., Zhu, J., Li, Y., Ladjadj, M., and Leith, A. (1996). SPIDER and WEB: processing and visualization of images in 3D electron microscopy and related fields. J. Struct. Biol. *116*, 190–199.

Gulick, A.M., Song, H., Endow, S.A., and Rayment, I. (1998). X-ray crystal structure of the yeast Kar3 motor domain complexed with Mg.ADP to 2.3 Å resolution. Biochemistry *37*, 1769–1776.

Hirose, K., Lockhart, A., Cross, R.A., and Amos, L.A. (1995). Nucleotide-dependent angular change in kinesin motor domain bound to tubulin. Nature *376*, 277–279.

Hirose, K., Cross, R.A., and Amos, L.A. (1998). Nucleotide-dependent structural changes in dimeric NCD molecules complexed to microtubules. J. Mol. Biol. *278*, 389–400.

Hirose, K., Löwe, J., Alonso, M., Cross, R.A., and Amos, L.A. (1999). Congruent docking of dimeric kinesin and ncd into three-dimensional electron cryomicroscopy maps of microtubule-motor ADP complexes. Mol. Biol. Cell *10*, 2063–2074.

Hirose, K., Henningsen, U., Schliwa, M., Toyoshima, C., Shimizu, T., Alonso, M., Cross, R.A., and Amos, L.A. (2000). Structural comparison of dimeric Eg5, Neurospora kinesin (Nkin) and Ncd head-Nkin neck chimera with conventional kinesin. EMBO J. *19*, 5308–5314.

Hoenger, A., Sack, S., Thormahlen, M., Marx, A., Muller, J., Gross, H., and Mandelkow, E. (1998). Image reconstructions of microtubules decorated with monomeric and dimeric kinesins: comparison with x-ray structure and implications for motility. J. Cell Biol. *141*, 419–430.

Hoenger, A., Thormahlen, M., Diaz-Avalos, R., Doerhoefer, M., Goldie, K.N., Muller, J., and Mandelkow, E. (2000). A new look at the microtubule binding patterns of dimeric kinesins. J. Mol. Biol. *297*, 1087–1103.

Howard, J. (2001). Mechanics of Motor Proteins and the Cytoskeleton (Sunderland, Massachusetts: Sinauer Associates, Inc.).

Jones, T.A., Zou, J.Y., Cowan, S.W., and Kjeldgaard. (1991). Improved methods for building protein models in electron density maps and the location of errors in these models. Acta. Crystallogr. A *47*(*Pt 2*), 110–119.

Kikkawa, M., Okada, Y., and Hirokawa, N. (2000). 15 Å resolution model of the monomeric kinesin motor, Kif1A. Cell *100*, 241–252.

Kikkawa, M., Sablin, E.P., Okada, Y., Yajima, H., Fletterick, R.J., and Hirokawa, N. (2001). Switch-based mechanism of kinesin motors. Nature *411*, 439–445.

Kozielski, F., De Bonis, S., Burmeister, W.P., Cohen-Addad, C., and Wade, R.H. (1999). The crystal structure of the minus-end-directed microtubule motor protein ncd reveals variable dimer conformations. Structure *7*, 1407–1416.

Kull, F.J., and Endow, S.A. (2002). Kinesin: switch I & II and the motor mechanism. J. Cell Sci. *115*, 15–23.

Kull, F.J., and Endow, S.A. (2004). A new structural state of myosin. Trends Biochem. Sci. *29*, 103–106.

Löwe, J., Li, H., Downing, K.H., and Nogales, E. (2001). Refined structure of alpha beta-tubulin at 3.5 Å resolution. J. Mol. Biol. *313*, 1045–1057.

Meluh, P.B., and Rose, M.D. (1990). KAR3, a kinesin-related gene required for yeast nuclear fusion. Cell *60*, 1029–1041.

Nitta, R., Kikkawa, M., Okada, Y., and Hirokawa, N. (2004). Kif1A alternately uses two loops to bind microtubules. Science *305*, 678–683.

Okada, Y., and Hirokawa, N. (2000). Mechanism of the single-headed processivity: diffusional anchoring between the K-loop of kinesin and the C terminus of tubulin. Proc. Natl. Acad. Sci. USA *97*, 640–645.

Ray, S., Meyhofer, E., Milligan, R.A., and Howard, J. (1993). Kinesin follows the microtubule's protofilament axis. J. Cell Biol. *121*, 1083–1093.

Reubold, T.F., Eschenburg, S., Becker, A., Kull, F.J., and Manstein, D.J. (2003). A structural model for actin-induced nucleotide release in myosin. Nat. Struct. Biol. *10*, 826–830.

Sablin, E.P., and Fletterick, R.J. (2001). Nucleotide switches in molecular motors: structural analysis of kinesins and myosins. Curr. Opin. Struct. Biol. *11*, 716–724.

Sablin, E.P., Case, R.B., Dai, S.C., Hart, C.L., Ruby, A., Vale, R.D., and Fletterick, R.J. (1998). Direction determination in the minus-end-directed kinesin motor ncd. Nature *395*, 813–816.

Sack, S., Kull, F.J., and Mandelkow, E. (1999). Motor proteins of the kinesin family. Structures, variations, and nucleotide binding sites. Eur. J. Biochem. *262*, 1–11.

Shipley, K., Hekmat-Nejad, M., Turner, J., Moores, C., Anderson, R., Milligan, R., Sakowicz, R., and Fletterick, R. (2004). Structure of a kinesin microtubule depolymerization machine. EMBO J. *23*, 1422–1432.

Song, H., and Endow, S.A. (1997). Rapid purification of microtubule motor domain proteins expressed in bacteria. Biotechniques *22*, 82–85.

Song, H., and Endow, S.A. (1998). Decoupling of nucleotide- and microtubule-binding sites in a kinesin mutant. Nature *396*, 587–590.

Tani, K., Sasabe, H., and Toyoshima, C. (1996). A set of computer programs for determining defocus and astigmatism in electron images. Ultramicroscopy *65*, 31–44.

Toyoshima, C. (2000). Structure determination of tubular crystals of membrane proteins. I. Indexing of diffraction patterns. Ultramicroscopy *84*, 1–14.

Vale, R.D., and Milligan, R.A. (2000). The way things move: looking under the hood of molecular motor proteins. Science *288*, 88–95.

Wendt, T.G., Volkmann, N., Skiniotis, G., Goldie, K.N., Muller, J., Mandelkow, E., and Hoenger, A. (2002). Microscopic evidence for a minus-end-directed power stroke in the kinesin motor ncd. EMBO J. *21*, 5969–5978.

Yun, M., Zhang, X., Park, C.G., Park, H.W., and Endow, S.A. (2001). A structural pathway for activation of the kinesin motor ATPase. EMBO J. *20*, 2611–2618.

Yun, M., Bronner, C.E., Park, C.G., Cha, S.S., Park, H.W., and Endow, S.A. (2003). Rotation of the stalk/neck and one head in a new crystal structure of the kinesin motor protein, Ncd. EMBO J. *22*, 5382–5389.